Turbulence Measurements with Acoustic Doppler Velocimeters

Carlos M. García[1]; Mariano I. Cantero[2]; Yarko Niño[3]; and Marcelo H. García[4]

Abstract: The capability of acoustic Doppler velocimeters to resolve flow turbulence is analyzed. Acoustic Doppler velocimeter performance curves (APCs) are introduced to define optimal flow and sampling conditions for measuring turbulence. To generate the APCs, a conceptual model is developed which simulates different flow conditions as well as the instrument operation. Different scenarios are simulated using the conceptual model to generate synthetic time series of water velocity and the corresponding sampled signals. Main turbulence statistics of the synthetically generated, sampled, and nonsampled time series are plotted in dimensionless form (APCs). The relative importance of the Doppler noise on the total measured energy is also evaluated for different noise energy levels and flow conditions. The proposed methodology can be used for the design of experimental measurements, as well as for the interpretation of both field and laboratory observations using acoustic Doppler velocimeters.

DOI: 10.1061/(ASCE)0733-9429(2005)131:12(1062)

CE Database subject headings: Flow measurement; Doppler systems; Turbulent flow; Filters; Noise.

Introduction

Present day laboratory and field research in fluid dynamics often requires water velocity measurements with a high temporal and spatial resolution. Laser Doppler velocimetry (LDV) and particle image velocimetry (PIV) have become the most common measuring techniques used in laboratory studies that satisfy such requirements. However, the feasibility of using these techniques is reduced when the scale of the experiment increases. The use of PIV/LDV may also be unsuitable in flows with suspended sediment concentrations. On the other hand, the use of hot wire anemometers, which provides a very good temporal resolution, is rather limited when impurities are present in the water, thus precluding applications with sediment transport or where it becomes difficult to control water quality that render the flow opaque. In most of these cases, acoustic Doppler velocimetry is the technique of choice, because it is relatively low in cost, can record at a relatively high frequency (up to 100 Hz), and has a relatively small sampling volume (varies from 0.09 to 2 cm^3 according to the instrument selected). Additionally, the measurements are performed in a remote control volume (located between 5 to 18 cm from the sensor according to the instrument selected), which reduces the interference with the flow being measured. ADV and NDV are trademark names for acoustic Doppler velocimeters manufactured by Sontek and Nortek, respectively.

Acoustic Doppler velocimeters are capable of reporting accurate mean values of water velocity in three directions (Kraus et al. 1994; Lohrmann et al. 1994; Anderson and Lohrmann 1995; Lane et al. 1998; Voulgaris and Trowbridge 1998; Lopez and García 2001), even in low flow velocities (Lohrmann et al. 1994). However, the ability of this instrument to accurately resolve flow turbulence is still uncertain (Barkdoll 2002).

Lohrmann et al. (1994) argued that the acoustic Doppler velocimeters resolution is sufficient to capture a significant fraction of the turbulent kinetic energy (TKE) of the flow. However, they identified the Doppler noise as a problem that causes the TKE to be biased toward a high value. Anderson and Lohrmann (1995) detected a flattening of the power spectrum of the velocity signal due to this Doppler noise, this suggests that an operational noise is eventually reached where the higher-frequency components of the signal cannot be resolved adequately.

Most research related to the capability of acoustic Doppler velocimeters to resolve the flow turbulence (specifically TKE and spectra) has focused on definition of the noise level present in the signal and how it can be removed (Lohrmann et al. 1994; Anderson and Lohrmann 1995; Lane et al. 1998; Nikora and Goring 1998; Voulgaris and Trowbridge 1998; Lemmin and Lhermitte 1999; McLelland and Nicholas 2000). However, little attention has been dedicated to evaluating the filtering effects of the sampling strategy (spatial and temporal averaging) on the turbulent parameters (moments, spectra, autocorrelation functions, etc.). Only the paper by Voulgaris and Trowbridge (1998) discusses some issues related to the effect of spatial averaging on turbulence measurements.

[1]Research Assistant, Ven Te Chow Hydrosystems Laboratory, Dept. of Civil and Environmental Engineering, Univ. of Illinois at Urbana–Champaign, 205 North Mathews Ave., Urbana, IL 61801. E-mail: cgarcia2@uiuc.edu

[2]Research Assistant, Ven Te Chow Hydrosystems Laboratory, Dept. of Civil and Environmental Engineering, Univ. of Illinois at Urbana–Champaign, 205 North Mathews Ave., Urbana, IL 61801. E-mail: mcantero@uiuc.edu

[3]Associate Professor, Dept. of Civil Engineering, Univ. of Chile, Casilla 228-3, Santiago, Chile. E-mail: ynino@ing.uchile.cl

[4]Chester and Helen Siess Professor, and Director, Ven Te Chow Hydrosystems Laboratory, Dept. of Civil and Environmental Engineering, Univ. of Illinois at Urbana–Champaign, 205 North Mathews Ave., Urbana, IL 61801. E-mail: mhgarcia@uiuc.edu

Note. Discussion open until May 1, 2006. Separate discussions must be submitted for individual papers. To extend the closing date by one month, a written request must be filed with the ASCE Managing Editor. The manuscript for this paper was submitted for review and possible publication on April 6, 2004; approved on March 23, 2005. This paper is part of the ***Journal of Hydraulic Engineering***, Vol. 131, No. 12, December 1, 2005. ©ASCE, ISSN 0733-9429/2005/12-1062–1073/ $25.00.

The capability of acoustic Doppler velocimeters to resolve flow turbulence is analyzed herein by means of a new tool, termed the acoustic Doppler velocimeter performance curves (APCs). These curves can be used to define optimal flow and sampling conditions for turbulence measurements using this kind of velocimeters. The performance of these tools is validated herein using experimental results. The APCs are used to define a new criterion for good resolution measurements of the flow turbulence. In cases where this criterion cannot be satisfied, these curves can be used to make appropriate corrections.

Another set of curves are also introduced to evaluate the relative importance of the Doppler noise energy on the total measured energy. In cases where the noise is significant, the noise energy level needs to be defined and corrections to the turbulence parameters (e.g., TKE, length and time scales, and convective velocity) must be performed.

Principle of Operation of Acoustic Doppler Velocimeters

An acoustic Doppler velocimeter measures three-dimensional flow velocities using the Doppler shift principle, and the instrument consists of a sound emitter, three sound receivers, and a signal conditioning electronic module. The sound emitter generates an acoustic signal that is reflected back by sound-scattering particles present in the water, which are assumed to move at the water's velocity. The scattered sound signal is detected by the receivers and used to compute the Doppler phase shift, from which the flow velocity in the radial or beam directions is calculated. A detailed description of the velocimeter operation can be found in McLelland and Nicholas (2000). In the present paper, a brief description of the instrument characteristics is included to facilitate presentation of a suitable conceptual model for the objectives detailed above.

The acoustic Doppler velocimeter uses a dual pulse-pair scheme with different pulse repetition rates, τ_1 and τ_2, separated by a dwell time τ_D (McLelland and Nicholas 2000). The longer pair of pulses is used for higher precision velocity estimates, while the shorter pulse is used for ambiguity resolution, assuming that the real velocity goes beyond the limit resolvable by the longer time lag. These pulse repetition rates can be adjusted by changing the velocity range of the measurement. Each pulse is a square-shaped pulse train of an acoustic signal (the frequency can be 5, 6, 10, or 16 MHz, depending on the instrument selected). The phase shift is calculated from the auto- and cross correlation computed for each single pulse-pair using pulse-to-pulse coherent Doppler techniques (Lhermitte and Serafin 1984). The radial velocities v_i (i=1,2,3) are computed using the Doppler relation

$$v_i = \frac{C}{4\pi f_{\mathrm{ADV}}} \left.\frac{d\phi}{dt}\right|_i \tag{1}$$

where C=speed of the sound in water; f_{ADV}=sound signal frequency (10 MHz); and $d\phi/dt|_i$=phase shift rate computed for receiver i. The radial or beam velocities are then computed sequentially for each receiver and, thus the time it takes to complete a three-dimensional velocity measurement is given by

$$T = 3(\tau_1 + \tau_D + \tau_2 + \tau_D) \tag{2}$$

This process is conducted with a frequency f_S (equal to $1/T$), which is between 100 and 263 Hz depending on the velocity range and the user-set frequency f_R (see Table 1). Then, the radial or beam velocities are converted to a local Cartesian coordinate system (u_x, u_y, u_z) using a transformation matrix that is determined empirically (through calibration) by the manufacturer (e.g. McLelland and Nicholas 2000).

Table 1. Frequencies Used by Acoustic Doppler Velocimeter

	f_R [Hz]	1	25	100
Velocity range (cm/s)	$f_{\text{cut-off}}$ [Hz]	0.44	11.3	50
			f_S (Hz)	
250		263	250	200
100		256	225	200
30		226	200	100
10		180	175	100
3		143	125	100

During the time it takes to make a three-dimensional velocity measurement, the flow may vary, however, these high-frequency variations are smoothed out in the process of signal acquisition and, therefore, cannot be captured by the instrument. Each radial velocity, v_i, is the result of the acoustic echo reflected by the sound-scattering particles in the water during an overall time $T/3$, and this is hence an average value of the real flow velocity in this time interval. Also, each of the final Cartesian velocity components is an average of the three radial velocity components (the product of the transformation matrix and the radial velocity). The direct implication of these features is that the Cartesian flow velocity represents an averaged value, over an interval time T, of the real flow velocity. In this sense T can be considered as the instrument response time, and the process of acquisition itself can be seen as an analog filter with a cut-off frequency, $1/T$ (or f_S). The time averaging process is analogous to the spatial averaging of the recorded velocity vectors that occurs within the measurement volume.

Two main conclusions can be drawn from the considerations above. First, energy in the signal with a frequency higher than f_S is filtered out (i.e., acquisition process acts as a low-pass filter). Second, aliasing of the signal occurs since the velocity signal is sampled at a frequency f_S, and the highest frequency that can be resolved by the instrument is $f_S/2$ [Nyquist theorem, see Bendat and Piersol (2000)]. This indicates that energy in the frequency range of $f_S/2 < f < f_S$ is folded back into the range $0 < f < f_S/2$, which may or may not be of importance depending on the flow characteristics. Flows with a large convective velocity, U_c, will have a considerable portion of the energy in the range of wavelengths: $f_S/(2U_c) < f/U_c < f_S/U_c$, while flows with a low convective velocity will have no energy in this range and, therefore, aliasing will not be of relevance.

After the digital velocity signal is obtained (with frequency f_S), the instrument performs an average of N values to produce a digital signal with frequency $F_R = f_S/N$, which is the acoustic Doppler velocimeter's *user-set frequency* with which velocity data are recorded. This averaging process is a digital nonrecursive filter (Hamming 1983; Bendat and Piersol 2000), the consequences of which are analyzed next.

Implications of Digital Averaging of Velocity Signals

Let x be the signal sampled at f_S and let y be the signal obtained after digital averaging (with frequency f_R). The interval between samples of signal x is $\Delta t_x = 1/f_S$ and between samples of signal y is $\Delta t_y = 1/f_R$ (see Fig. 1) Notice that $f_S = N f_R$.

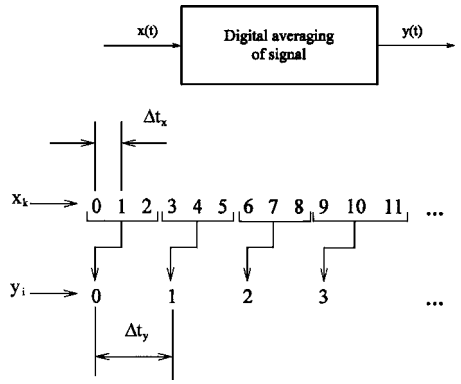

Fig. 1. Digital averaging of water velocity signal for $N=3$. Acoustic Doppler velocimeter acquires a water velocity signal x at frequency f_S and then processes it (digital averaging) into y which is the velocity signal recorded at frequency f_R ($f_S=N\,f_R$, $\Delta t_x=1/f_S$, and $\Delta t_y=1/f_R$).

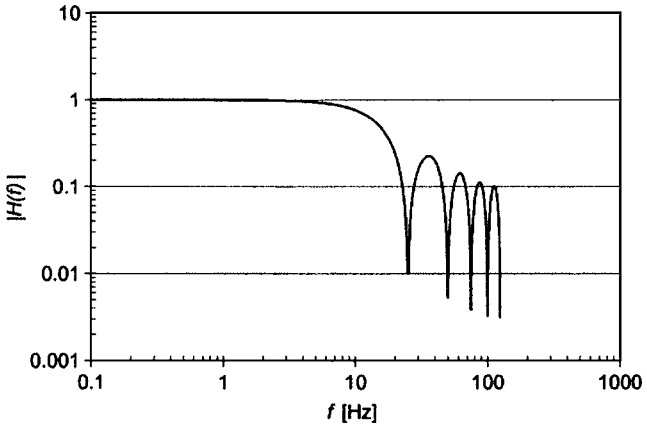

Fig. 2. Gain factor of the nonrecursive digital filter for $f_R=25$ Hz and $f_S=250$ Hz. The cut-off frequency $f_{\text{cut-off}}$ of the filter is defined as the frequency for which the gain factor equals $\sqrt{2}/2$.

The nonrecursive digital filter is given by

$$y_i=\sum_{n=0}^{N-1}\frac{1}{N}x_{Ni+n} \tag{3}$$

or in the time domain

$$y(t)=\sum_{n=0}^{N-1}\frac{1}{N}x\left(t+\frac{n}{N\,f_R}\right) \tag{4}$$

where $t=i\,\Delta t_y=N\,i\,\Delta t_x$. The transfer function of this filter, $H(f)$, can be calculated by computing the Fourier transform of Eq. (4), i.e.

$$H(f)=\frac{Y(f)}{X(f)}=\sum_{n=0}^{N-1}\frac{\exp\left(j2\pi\dfrac{nf}{N\,f_R}\right)}{N} \tag{5}$$

where $Y(f)$ and $X(f)$=Fourier transforms; and $j=(-1)^{1/2}$. The sum in Eq. (5) can be computed to give

$$H(f)=\frac{f_R}{f_S}\frac{\exp\left(j2\pi\dfrac{f}{f_R}\right)-1}{\exp\left(j2\pi\dfrac{f}{f_S}\right)-1} \tag{6}$$

noting that $Nf_R=f_S$. The gain factor of the filter is

$$|H(f)|=\frac{f_R}{f_S}\sqrt{\frac{1-\cos\left(2\pi\dfrac{f}{f_R}\right)}{1-\cos\left(2\pi\dfrac{f}{f_S}\right)}} \tag{7}$$

Fig. 2 shows the gain factor $|H(f)|$ for $f_R=25$ Hz and $f_S=250$ Hz. The cut-off frequency $f_{\text{cut-off}}$ of the filter is defined as the frequency for which the gain factor equals $\sqrt{2}/2$. The cut-off frequency must be equal to or smaller than the Nyquist frequency ($f_R/2$) in order to avoid significant aliasing. Cut-off frequencies of the digital filter applied by acoustic Doppler velocimeters for different velocity ranges are presented in Table 1.

As observed in Fig. 2, the gain factor possesses some lobes after the cut-off frequency that could generate some energy aliasing. This could be improved in the acoustic Doppler velocimeter design by performing a different digital filtering of the signal in the decimation process so that the data are reduced from f_S to f_R.

Conceptual Model

A conceptual model is developed here to evaluate the performance of the acoustic Doppler velocimeter based on turbulence characteristics of the flows to be measured. The model consists of two components, for the instrument and the flow, which simulate the instrument operation (based on the previous description of how the velocimeter works) and the power spectrum of flow velocities associated with different flow conditions. A description of each component is presented next.

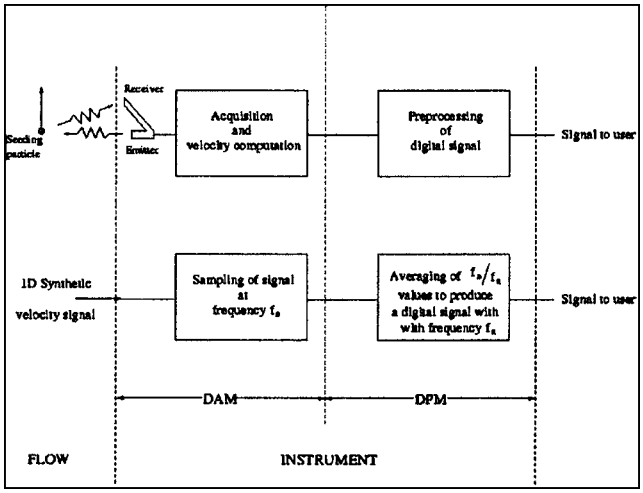

Fig. 3. Conceptual model for instrument functioning as a two-module linear system. The first module is the data acquisition module which models the velocity sampling at frequency f_S and the computation of flow velocities from the acquired signal. The second module is the data preprocessing module which models the digital averaging processing.

Instrument Component

For the purpose of this work, the acoustic Doppler velocimeter can be conceptually modeled as a two-module linear system (Fig. 3). The first module is the data acquisition module (DAM), which encompasses the sound emitter and receivers, the analog to digital converter (which works at frequency f_S), and the computation of flow velocities from the acquired signal. The second module is the data preprocessing module (DPM), which encompasses the averaging of the digital velocity signal that produces data at the user-set frequency f_R.

The DAM produces a digital signal with frequency f_S (signal x in the analysis of previous section) from the input flow velocity. This module is modeled through the sampling of synthetic water velocity series produced in the flow component of the conceptual model. The DPM basically performs a time averaging of the output of the DAM in order to produce data at the user-set frequency f_R. This module is modeled by Eq. (3). The output is the digital signal of water velocity.

Although the low-pass filtering of the signal (in the DPM) is mandatory to avoid aliasing, it has implications in the computation of the spectrum and moments from the signal. Its effect in the spectrum is clear since the low-pass filter removes energy beyond the cut-off frequency. In the case of a perfect low-pass filter, the energy content of the spectrum vanishes at frequencies larger than the cut-off frequency of the DPM (Roy et al. 1997). Likewise, the low-pass filter reduces the values of the even moments of the signal. The quantification of this effect is discussed later in this paper.

Flow Component

Synthetic signals of water velocity need to be generated to represent different ranges of flow conditions, and must have turbulence characteristics that resemble realistic conditions. In order to accomplish this, a one-dimensional (1D) model power spectrum E_{11} was adopted that includes all of the turbulence characteristics for specified flow conditions. The model power spectrum used in this paper [Eq. (8)] is based on that proposed by Pope (2000). The input parameters of the model are the energy-containing eddy length scale, L, and Kolmogorov length scale η (which can be estimated from the value of the rate of dissipation of TKE, ε)

$$E_{11}(\kappa_1) = C_0 \varepsilon^{2/3} \kappa_1^{-5/3} f_L(\kappa_1 L) f_\eta(\kappa_1 \eta) \tag{8}$$

where C_0=constant; κ_1=wave number; and f_L and f_η=shape functions defined as

$$f_L(\kappa_1 L) = \left(\frac{\kappa_1 L}{\left[(\kappa_1 L)^2 + c_L \right]^{1/2}} \right)^{5/3+p_0} \tag{9}$$

$$f_\eta(\kappa_1 \eta) = \exp\left\{ -\beta \left\{ \left[(\kappa_1 \eta)^4 + c_\eta^4 \right]^{1/4} - c_\eta \right\} \right\} \tag{10}$$

Here, p_o, c_L, c_η, and β=parameters of the shape functions. The function f_L defines the shape of the energy-containing part of the spectrum (equal to 1 for large $\kappa_1 L$). On the other hand f_η describes the shape of the dissipation range (equal to 1 for small $\kappa_1 \eta$). Following Pope (2000), the parameters finally adopted for this model were: C_0=0.49, p_0=0, c_L=6.78, c_η=0.40, and β=5.2.

A technique is needed to generate synthetic water velocity signals from the modeled 1D power spectrum with predefined turbulence flow conditions. For this, the method of Shinozuka and Jan (1972) is used, which allows a random 1D water velocity signal to be generated as a realization of a turbulent process, using the model power spectrum as a target. Each point in the time series is computed by summing the weighted cosine series with a random phase angle, ϕ, as

$$x(t) = \sqrt{2} \sum_{q=1}^{Ns} A_q \cos(\omega_q' t + \phi_q) \tag{11}$$

The generated synthetic signal is only one of the possible realizations of a process with the chosen flow turbulence characteristics because of its random phase angle. The weights A_q are defined from the Ns numbers of terms of the target spectrum (computed before)

$$A_q = \left[E_{11}(\omega_q) \Delta\omega \right]^{1/2} \tag{12}$$

Here ω_q, ω_q', and $\Delta\omega$ are obtained from Taylor's frozen turbulence approximation using the convective velocity U_c as

$$\omega_q = \kappa_{1_q} U_c; \quad \Delta\omega = \Delta\kappa_1 \cdot U_c \tag{13}$$

$$\omega_q' = \omega_q + \delta\omega \tag{14}$$

where $\delta\omega$=random frequency with a uniform probability density distribution in the range—$\alpha\Delta\omega/2$ *to* $\alpha\Delta\omega/2$. The parameter α is known as the amount of jitter ($\alpha \ll 1$) and Shinozuka and Jan (1972) suggested a value of α=0.05. Finally, the random phase angle, ϕ, has a uniform probability density distribution in the range from 0 to 2π.

Jeffries et al. (1991) suggested several recommendations regarding the method of Shinozuka and Jan (1972), consisting of requirements for Ns (number of terms of the target spectrum) and Nt (number of points in the time series) to avoid undesired periodicity in the synthetic signals. These suggestions were adopted herein, and the parameters used for the simulations are: Ns=32,768, total simulated time Tt=120 s, f_S=260.8 Hz, and Nt=31,291. Different values of $\Delta\kappa$ were used in order to yield a frequency f_S=260.8 Hz in all the runs, which is very close to the frequency at which the velocimeter samples the flow in the velocity range =250 cm/s. Both the model power spectrum and the method used to generate synthetic velocity series were tested and validated using experimental data.

Simulation of Different Flow Conditions Using the Conceptual Model

A set of numerical simulations based on the conceptual model was conducted for different values of the parameters in the range that best represents the conditions usually present in laboratory and field turbulence measurements. The ranges of flow variables used in the simulations are: Convective velocity=0.01 m/s $\leq U_c \leq$ 1 m/s; energy containing eddy length scale: 0.10 m $\leq L \leq$ 2 m; Kolmogorov length scale: 0.0001 m $\leq \eta \leq$ 0.005 m. The rate of dissipation of TKE, ε, is related to the Kolmogorov length scale using dimensional analysis (Pope 2000)

$$\varepsilon = \frac{\nu^3}{\eta^4} \tag{15}$$

The range of Kolmogorov length scales proposed here generates for a water temperature equal to 20°C ($\nu = 10^{-6}$ m^2/s), a range of seven orders of magnitude in ε (1.6×10^{-9} m^2/s$^3 \leq \varepsilon \leq 1 \times 10^{-2}$ m^2/s^3), thus describing conditions prevailing in most environmental water flows, from open-channel flows to lakes (Mercier 1984).

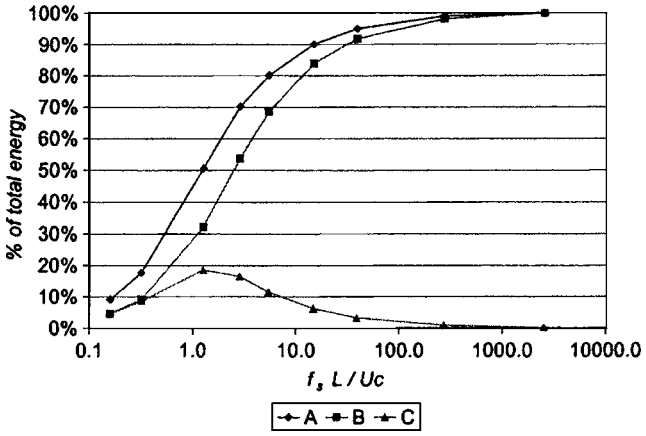

Fig. 4. Percentage of the energy remaining in the sampled signal for: Curve A: $f<f_S$; Curve B: $f<f_S/2$; and Curve C=energy corresponding to frequencies $f_S/2<f<f_S$

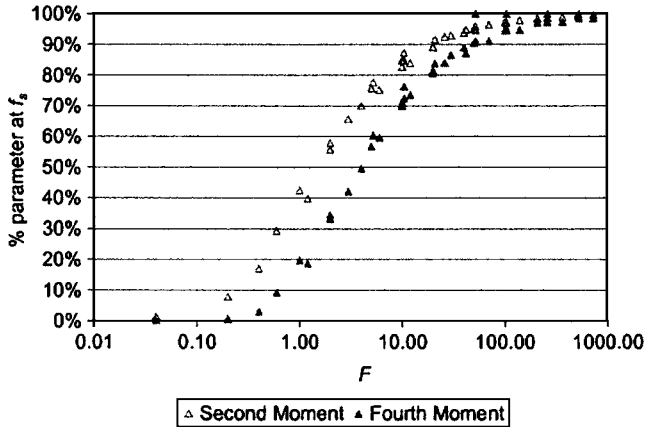

Fig. 5. Effects of digital averaging on second- and fourth-order moments of the water velocity signals. For $F=f_RL/U_c=20$, the second- and fourth-order moments of the signal sampled at frequency f_R are about 90 and 80%, respectively, of the values of the parameters of the signal sampled at frequency f_S.

Acoustic Doppler Velocimeter Performance Curves Sampling the Flow Turbulence

First, a set of 1D model spectra were computed for different flow conditions. These spectra were then integrated to compute flow energies and evaluate both the effects of the analog filter with cut-off frequency f_S, and the level of aliased energy with frequencies in the range $f_S/2\leqslant f<f_S$ in the original (unsampled) time series. Such energy is folded back through the sampling process and confused with resolved energy corresponding to frequencies in the range $0\leqslant f<f_S/2$.

The results obtained are shown in Fig. 4 in dimensionless form. As the dimensionless number f_SL/U_c increases, a smaller portion of the energy is both filtered and aliased. The poorest measurement conditions for the acoustic Doppler velocimeter in the range of parameters considered, are defined by extreme flow conditions (L=0.1 m and U_c=1 m/s, which combined yield a minimum value of f_SL/U_c at a given frequency) and the smaller velocimeter velocity range which can sample this convective velocity (equivalent to 1 m/s). For this velocity range, at f_R=25 Hz, the frequency f_S=225 Hz (see Table 1), and thus the value of the dimensionless number f_SL/U_c is 22.5. In such a case, the analog filter would take about 8.4% of the total energy out of the signal when it is sampled at f_S=225 Hz. Additionally, for frequencies equal to $f_S/2$, the accumulated energy would be 86.4% of the total energy in the flow, which implies that only 5.2% of the total energy will be aliased. The values cited before correspond to extreme conditions, and for lower values of U_c (corresponding to a lower velocity range) and, consequently, for lower values of f_S (see Table 1), the percentage of aliased energy should decrease. Based on the values cited before, it is concluded from the model behavior of the velocimeter that both the effects of the analog filter (with cut-off frequency f_S) and the level of aliased energy are lower than 10% even in the most critical conditions. Besides, the digital filtering performed by the DPM using a cut-off frequency smaller than $f_S/2$ takes most of the aliased energy out of the spectrum.

Next, a number of synthetic turbulent water velocity signals with Δt=0.0038 s (f_S=260.8 Hz) were generated as realizations of different flow conditions and then sampled according to the sampling strategy described in the instrument component of the conceptual model. The use of different values of f_S corresponding to different velocity ranges does not affect the results of the analysis performed herein, because the gain factor of the velocimeter digital filtering does not depend on the number of averaged values in the signal to produce the same user-defined frequency f_R. The *user-set frequencies* adopted here were f_R=260.8, 52.2, 26.1, 10, 5, and 3 Hz. The sampled signals were analyzed in order to compute corresponding turbulent parameters (up to fourth-order moments, autocorrelation function, power spectrum, and time scales). Thus, the variation of these parameters can be evaluated as flow conditions and sampling frequency change.

The effect of different flow conditions on the flow statistics is explored in Figs. 5–8. The parameters representing the flow statistics obtained for values $f_R\leqslant f_S$ are made dimensionless using the corresponding value of the parameter computed for $f_R=f_S$=260.8 Hz (no averaging). Those dimensionless parameters are plotted as a function of the dimensionless parameter F defined as

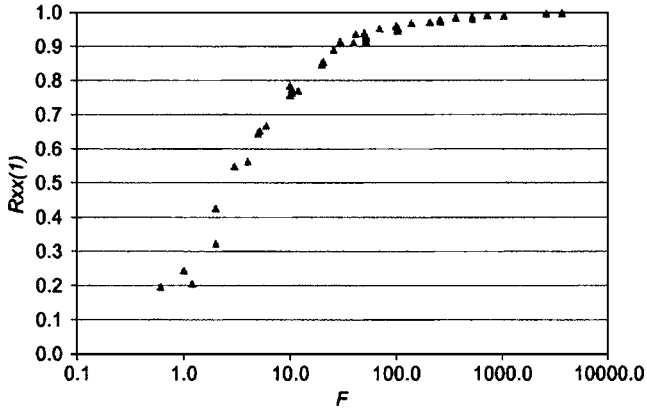

Fig. 6. Autocorrelation function values at Lag 1 of the recorded water velocity signal. Smaller values of $Rxx(1)$ mean that there is less turbulence sampled in these signals. For $F=f_RL/U_c=20$, $Rxx(1)$ is 0.85.

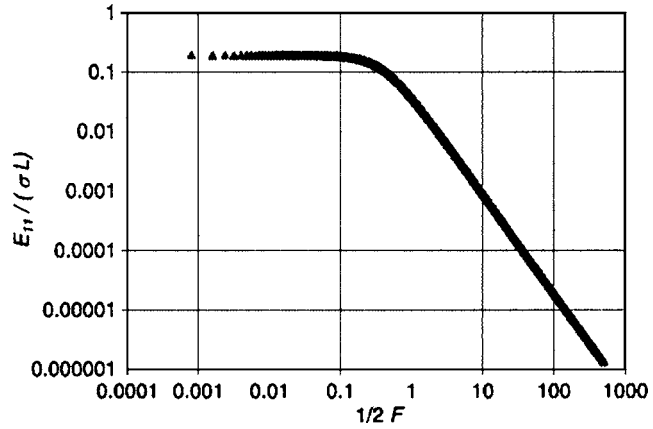

Fig. 7. Dimensionless power spectrum model. For $F=f_R L/U_c=20$, a good portion of the inertial range is resolved.

$$F=\frac{L}{\frac{U_c}{f_R}}=\frac{f_R}{f_T}=\frac{L}{d_R} \tag{16}$$

where f_T=characteristic frequency of large eddies present in the flow; and d_R=diameter of the sampled volume set by the flow and sampling characteristics. The higher the ratio F, the better the description of the turbulence that can be achieved with a specific instrument. In theory, no turbulence scale could be described from the recorded signal for $F<1$.

So far, the sampling volume has been considered as a point. However, spatial averaging performed by acoustic Doppler velocimeters of the turbulence fluctuations in the longitudinal flow direction of a uniform flow should be considered when the value of d_R is smaller than the diameter of the measurement volume, d. For instance, in the case of the 10 MHz Nortek velocimeter (d=6 mm, and f_R=25 Hz), $d_R<d$ for convective velocities smaller than 15 cm/s. In those cases, d must be used in Eq. (16) instead of d_R because spatial averaging of the turbulence fluctuations becomes more important than the temporal averaging of the turbulence fluctuations. This replacement is based on the assumption that the spatial average of the turbulence fluctuations acts as a low-pass filter with wavelength =1/d. A similar analysis could be performed for the vertical spatial averaging when the value of d_R is smaller than the vertical size of the measurement volume, d_v. The assumption included here is that a uniform longitudinal velocity profile is present in the vertical direction, which is a limitation mainly in velocity measurements close to the bottom of a wall boundary layer, where high velocity gradients are present.

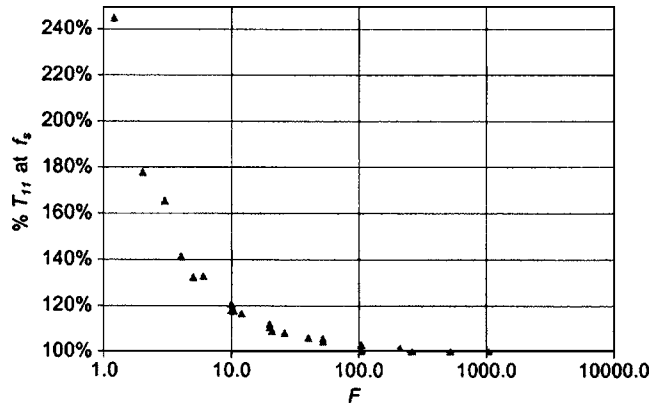

Fig. 8. Effects of digital averaging on integral time scale (T_{11}). For $F=f_R L/U_c=20$, T_{11} of the signal sampled at frequency F_R is about 110% of the values of the parameters of the signal sampled at frequency f_S.

The evolution of the variance (integral of the spectrum and second-order moment of the signal) is shown in dimensionless form in Fig. 5, together with the corresponding fourth-order moments. The effects of the averaging on the fourth-order moments is more important (i.e., higher reduction in the sampled moment) than on the variance. A similar analysis was performed for the third-order moments but a clear trend could not be detected. This is due to the fact that the third-order moment (as well as all the odd moments) usually presents a very small value, which requires a very long integration time to estimate them with a reasonable level of accuracy (Sreenivasan et al. 1978). If the skewness is exactly zero, the integration time required is indeterminate.

Analysis of the autocorrelation function at the first lag $R_{xx}(1)$, and the power spectrum E_{11} (included in Figs. 6 and 7, respectively) gives good information about how the sampling technique used by acoustic Doppler velocimeter affects the turbulence description. The spectrum is made dimensionless in Fig. 7 using the variance of the signal, σ, and the length scale of large eddies, L and plotted as a function of 1/2 F, because the maximum frequency represented in the spectrum is $f_R/2$. The first sampled point in the autocorrelation function (Fig. 6) decreases as f_R decreases. Smaller values of $Rxx(1)$ mean that there is less turbulence sampled in these signals and only a small zone of the inertial range is resolved in the power spectrum (Fig. 7). For $F=f_R L/U_c<1$, the inertial range is not resolved and $Rxx(1)=20\%$. As $F>2$, progressively more of the inertial range gets sampled but the value $Rxx(1)$ is still small unless F exceeds a value of about 20. The decorrelations for lags in the range from 0 to 1 (Fig. 6) are produced only for the flow conditions and sampling strategy considered here. Additionally, no noise effects are considered in the computation which would generate an extra level of decorrelation in the signal. The time scales computed from the autocorrelation function (as the integral of Rxx up to the first zero crossing) are biased to high values due to the sampling averaging. Fig. 8 quantifies this bias, showing the variation of this time scale with F in dimensionless terms.

Figs. 5–8 are called APCs, and yield criteria for sampling turbulence in water flows with ADV technology. From the present analysis, it is concluded that a good sampling criterion should consider values of $F>20$, since such a range yields reasonably small losses in the moments but at the same time resolves important portions of the spectrum. The limit $F=20$ means, for example, that when using an acoustic Doppler velocimeter with $f_R=25$ Hz for an experiment with $L=20$ cm, turbulence cannot be accurately resolved in flows with velocities higher than 25 cm/s. Nezu and Nakagawa (1993) empirically proposed a criterion to determine the maximum response frequency of a turbulence measuring device which allows analysis of the spectral distribution of the flow down to the viscous subrange. The maximum response frequency required in this analysis was chosen to satisfy the dimensionless number $F=16.67$ which agrees well with the value proposed here. However, the criterion empirically proposed by Nezu and Nakagawa (1993) concerns just open-channel flow conditions where L is the water depth and U_c is equal to the longitudinal velocity.

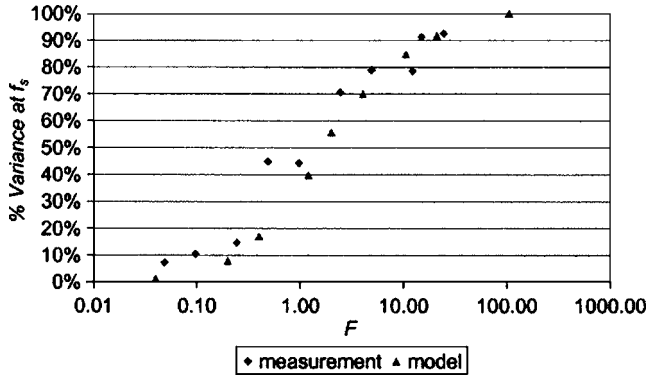

Fig. 9. Comparison between observed and predicted digital averaging effect on the variance of the recorded water velocity signal

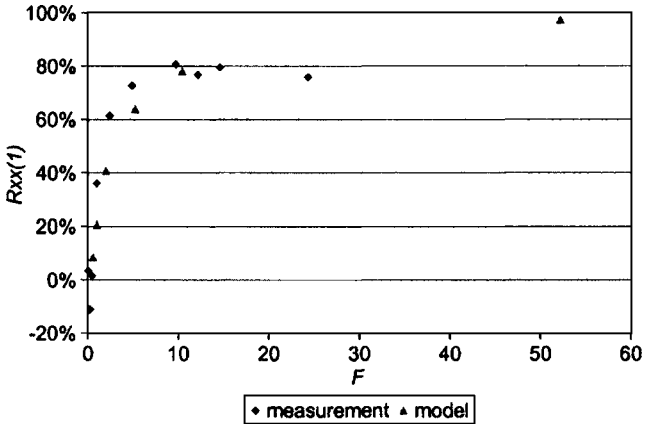

Fig. 11. Comparison between observed and predicted autocorrelation function value at Lag 1 of the recorded water velocity signal

Validation of the Acoustic Doppler Velocimeter Performance Curves

The assumptions used to develop the conceptual model are now validated using experimental data from an open-channel flow, recorded in a flume having a width $B=0.91$ m at the Ven Te Chow Hydrosystems Laboratory, University of Illinois at Urbana–Champaign (UIUC). First, a set of 11 three-dimensional water velocity time series were obtained with a down-looking Sontek Micro ADV (sampling volume 5 cm away from the probe) at the same location, flow conditions and instrument velocity range, but with different sampling frequencies (values of $f_R=50$; 30; 25; 20; 10; 5; 2; 1; 0.5; 0.2; 0.1 Hz). The longitudinal water velocity signals recorded for each configuration were used to develop Figs. 9–12. The quality of the recorded signals is characterized by a correlation value in the range from 82 to 93 and a signal to noise ratio (SNR) value in the range 17.9 to 22.9 dB, which are high enough values of these parameters to ensure good quality data. Water velocity signals were recorded for 2 min at each instrument configuration. The sampling volume of the velocimeter was located at $y_p=0.04$ m from the bottom of the flume. The flow condition analyzed consisted of a water depth $h=0.282$ m, flow discharge $Q=0.12$ (m^3/s), and a local value of the shear velocity at this vertical, $u^*=0.0482$ m/s. The scale of the energy containing eddies, L, corresponding to this flow is estimated to be equal to the depth=0.282 m, and the associated convective velocity is determined to be equal to $U_c=0.58$ m/s, from the three-dimensional velocity vector data using the relation proposed by Heskestad (1965)

$$U_{c1}^2 = U_1^2\left[1 + 2\frac{U_2^2}{U_1^2} + 2\frac{U_3^2}{U_1^2} + \frac{\overline{u_1'^2}}{U_1^2} + 2\frac{\overline{u_2'^2}}{U_1^2} + 2\frac{\overline{u_3'^2}}{U_1^2}\right] \quad (17)$$

where U_i and u_i'=mean and the fluctuation of the flow velocity in the i Cartesian direction. Following Nezu and Nakagawa (1993), the dimensionless parameter $\varepsilon h/u^{*3}$ is estimated to have a value equal to 16 for $y_p/h=0.142$. Thus, the rate of dissipation of TKE at the measurement point is 6.35×10^{-3} m^2/s^3 and the corresponding Kolmogorov length scale is 0.00011 m.

The evolution of second- and fourth-order moments of the measured velocity signals as f_R varies is plotted in Figs. 9 and 10, respectively. The values of the moments corresponding to the real sampling frequency, f_S, of the instrument are needed to make the plot dimensionless; however, this information cannot be obtained from the acoustic Doppler velocimeters. To overcome this problem, the value of the ratio between the corresponding moments obtained at f_R and f_S for the higher sampling frequency ($f_R=50$ Hz and $F=24.31$) is assumed to be the same as that predicted by the conceptual model (92.5% for the variance and 83%

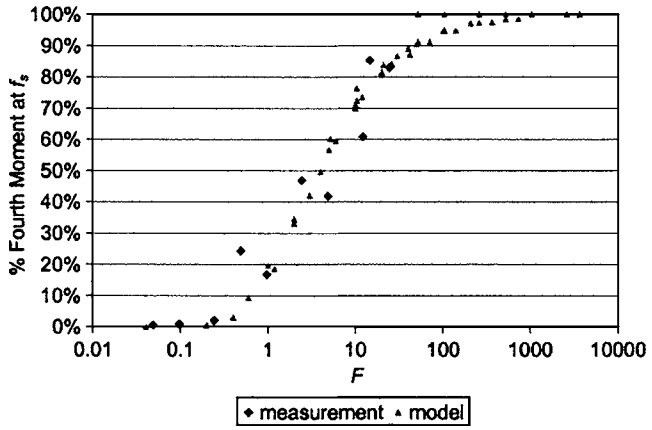

Fig. 10. Comparison between observed and predicted digital averaging effect on the fourth-order moment of the recorded water velocity signal

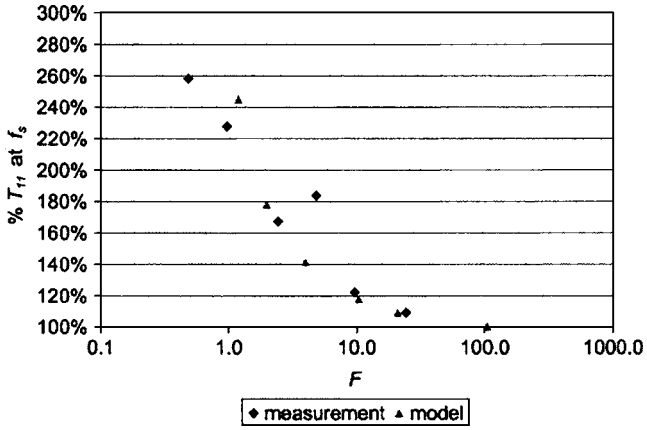

Fig. 12. Comparison between observed and predicted digital averaging effect on integral time scale (T_{11}) of the recorded water velocity signal

Table 2. Characteristics of the Experiments

Experiment no.	Flow conditions		Instrument	
	L (cm)	U_c (cm/s)	Type	f_R (Hz)
1	20	~43	Micro ADV Sontek	10
2	38	5–7	Micro ADV Sontek	25
3	50–60	15–23	Nortek NDV 10 MHz	25
4	85	17–22	ADV Sontek	25
5	365.8	~10	Nortek NDV 10 MHz	25
6	26.7	56–71	Micro ADV Sontek	25
7	28.2	58	Micro ADV Sontek	25
8	80	5–9	Micro ADV Sontek	25
9	700	12–13	Nortek NDV 10 MHz	10
10	15	10–21	ADV Sontek	25

for the fourth-order moment). The trend obtained from the measurements agrees very well with that predicted by the model (Figs. 9 and 10). The poor resolution of turbulence in the analyzed flow obtained with low sampling frequencies is shown by these figures by the fact that all of the even moments of the sampled frequencies are biased to low values. For instance, at frequency $f_R=1$ Hz ($F=f_RL/U_c=0.4862$), the recorded signal captured only 48.5 and 24% of the variance and fourth-order moment, respectively.

A good agreement is also obtained between measurements and the predictions of the conceptual model for the variation of the correlation value at the first lag, $Rxx(1)$ with the dimensionless frequency F (Fig. 11). The observed values of $Rxx(1)$ reach a rather constant value of about 80% at high frequencies due to the noise decorrelation. Fig. 12 shows the observed variation of the integral time scale with F. A good agreement is obtained between the prediction of the conceptual model and the observations, with exception of the behavior at dimensionless frequencies lower than about unity.

Further validation of the conceptual model was obtained by using water velocity signals recorded at several facilities by researchers at the Ven Te Chow Hydrosystems Laboratory of the UIUC since 1994. Corresponding experimental conditions are described in Table 2. The flow generated in an annular flume was analyzed in Experiment 1; open-channel flow conditions were simulated in three different tilting flumes for Experiments 2–5; in Experiment 6, water velocities signals were recorded in an experimental pool and riffle sequence with and without the presence of vegetation, respectively; flow velocity fields around bubble plumes were measured in Experiments 8 and 9 in a square and round tank, respectively; and finally, flow velocity signals recorded at points located inside a turbidity current were analyzed in Experiment 10. Experiment 7 is the source of data for the set of 11 time series used in Figs. 9–12. For the sake of clarity, only two points of this set are used in Fig. 13. These time series correspond to values of $F=12.02$ and $F=24.3$. The data included in Fig. 13 correspond only to velocity signals of the X Cartesian component from all of the experiments. This component was always aligned with the main flow direction. In all cases, the instrument was used in a down-looking orientation, with the exception of Experiments 3, 8, and 9, where a side-looking orientation was used. In summary, the quality of the recorded signals is characterized by correlation values in the range 84 to 99 and by SNR values in the range 18.6 to 30.20 DB.

Comparisons between the predicted and observed values of the autocorrelation function at Lag 1 for experimental conditions described in Table 2 are presented in Fig. 13. The decorrelation observed in the measured signals increases as the dimensionless number F decreases, in agreement with the predictions of the conceptual model. However, decorrelations that are higher than those predicted are observed due to noise effects, which are not accounted for by the theoretical APC curves. Based on this observation, it can be argued that these curves provide an upper limit of the actual ones.

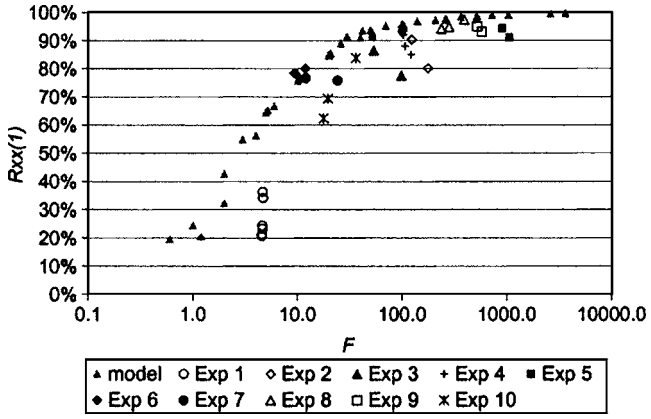

Fig. 13. Comparison between observed and predicted autocorrelation function value at Lag 1 of the recorded water velocity signals for different experimental conditions (see Table 2)

Noise Effects from Turbulence Parameters Computed from Acoustic Doppler Velocimeter Water Velocity Signals

The presence of noise in water velocity signals obtained using an acoustic Doppler velocimeter, and the techniques to reduce its effect in the computation of turbulence parameters obtained from these signals, have been the focus of several papers in recent years (Lohrmann et al. 1994; Nikora and Goring 1998; Voulgaris and Trowbridge 1998; McLelland and Nicholas 2000). Even when all of the possible precautions suggested by the manufacturers are taken into consideration (i.e., correlation, ρ, and SNR within defined ranges), the signal will have a noise level that affects the values of the turbulence parameters. Nikora and Goring (1998) and SonTek (1997) affirm that the main physical contributor to the acoustic Doppler velocimeter's noise is the Doppler noise. The Doppler noise has the characteristics of white noise (Nikora and Goring 1998; Lemmin and Lhermitte 1999; McLelland and Nicholas 2000) with a Gaussian probability distribution (Nikora and Goring 1998), as well as a flat power spectrum (Anderson and Lohrmann 1995) which indicates the presence of uncorrelated noise (Lemmin and Lhermitte 1999).

The fact that white noise presents the same energy level for all frequencies makes it impossible to subtract its effects from the temporal series using digital filters: however, its integral effects can be subtracted from some turbulence parameters. White noise does not affect the computation of the mean values because it has zero mean. Nikora and Goring (1998), Voulgaris and Trowbridge (1998), and McLelland and Nicholas (2000) showed that Reynolds stress computations are not affected by the presence of the white noise. Lohrmann et al. (1994) considered that the Reynolds stresses can be accurately determined even at levels below the

Doppler noise. Nikora and Goring (1998) claim that estimates of TKE are limited by the Doppler noise because the TKE is biased to high values. However, Lohrmann et al. (1994), Nikora and Goring (1998), and Gordon and Cox (2000) affirm that the contributions of noise over the total energy can be considered negligible for flows with high levels of turbulence, such as open-channel flow boundary layers.

The Doppler noise produces decorrelation of the signal and hence the autocorrelation function reduces its value to zero faster than in signals without noise. Consequently, the temporal scales obtained from this function are biased to low values. On the other hand, velocity spectra for the horizontal velocity components are biased toward high values due to the presence of the Doppler noise, while for the vertical velocity the noise is negligible (Lohrmann et al. 1994; Nikora and Goring 1998). Assuming that the noise and turbulent fluctuations are decorrelated (Nikora and Goring 1998), the spectrum of the resulting measurement is the sum of the turbulent spectrum plus the noise level. Nikora and Goring (1998) identified the Doppler noise as a flattening of the spectrum close to the Nyquist frequency, and found that in the worst case the flattening may take place around 4–5 Hz for the horizontal velocity but is more typically in the range of 5–10 Hz.

The main parameter used to subtract the Doppler noise effects on the turbulence parameters is the white noise energy level, the detection of which is discussed later. Using this level, the corrected power spectrum for each velocity component can be simply obtained by subtracting the white noise energy level from the measured spectra. Thus, by integrating the corrected power spectra, the corrected variances for each component, and from these the corrected TKE are computed. Additionally, the inverse fast Fourier transform of the corrected power spectrum can be used to estimate the autocorrelation function and associated corrected time scales can be obtained.

Detection of the Doppler Noise Energy Level

In a low-energy flow, the energy level of the white noise can be identified in a power spectrum as a flat plateau at high frequencies. Nikora and Goring (1998) suggested that the empirical spectra of the Doppler noise can be replaced by straight horizontal lines whose ordinates are equal to the average of the noise spectral ordinates. This technique was called "spectral analysis" by Voulgaris and Trowbridge (1998), who calculated the noise energy using the noise energy level detected in the tail of the spectrum (the frequency range is chosen so that there are ten estimates for the calculation of the statistically significant average, i.e., 11.5–12.5 Hz for sampling frequency=25 Hz).

Nikora and Goring (1998) identified a characteristic frequency, f_n, that demarks a boundary in the power spectrum between two regions. The first region corresponds to frequencies smaller than f_n, where the turbulence energy is much larger than the noise energy. In the other region, for frequencies higher than f_n, turbulence energy is weaker than the noise energy. If the frequency f_n is smaller than the Nyquist frequency ($f_R/2$), the flat plateau in the spectrum would be visualized. In these cases, the spectral analysis technique of Voulgaris and Trowbridge (1998) can be applied to estimate the noise energy level. Although this method becomes a very good approximation to determine the noise energy level, for high-energy flows the plateau cannot be distinguished in the spectrum, although this does not imply that the signal does not have intrinsic noise. In these cases, different methodologies have been suggested to estimate the noise level (Nikora and Goring 1998; Voulgaris and Trowbridge 1998; McLelland and Nicholas 2000), which all have some intrinsic difficulties. These methods mainly assume that the noise level of the signal is the same if the instrument configuration and flow conditions do not change. This implies that the users are recording signals with the same quality each time that the instrument is sampling the same flow conditions with the same configuration (sampling frequency, velocity range, etc.). However, there are certain conditions that cannot be controlled by the users during the measurement (for example, level of seeding particles, and bubbles attached to the sensor) which strongly affect the quality of the signal (Nikora and Goring 1998; Lemmin and Lhermitte 1999), and thus the noise level. SonTek (1997) suggested that estimation of the Doppler noise from a pulse coherent system [as Voulgaris and Trowbridge (1998), McLelland and Nicholas (2000) do] is a complicated operation, which for practical systems provides at best a lower bound for instrument noise level.

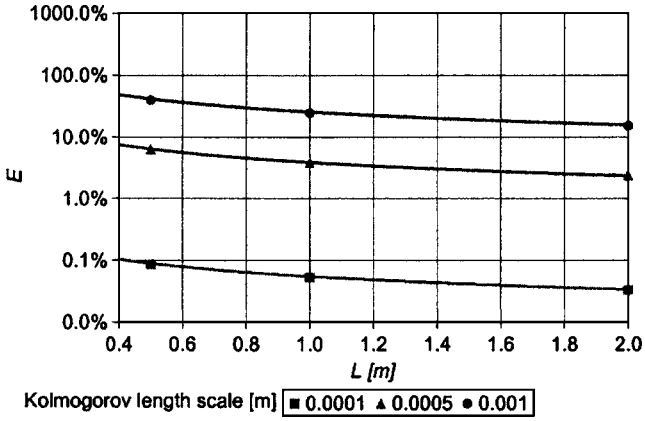

Fig. 14. Ratio between the noise energy and the real turbulent energy, E, for $U_c=0.5$ m/s, $f_R=25$ Hz, and $E_{11n}=10^{-6}$ m^2/s. Flow conditions with $L<0.4$ m ($F<20$) are disregarded in the analysis because of the requirements suggested by acoustic Doppler performance curves.

Evaluation of the Doppler Noise Effect on the Total Turbulent Energy

Some tools are introduced here to evaluate the relative importance (E) of the noise energy over the real turbulent energy for different flow conditions. E is defined as

$$E=\frac{(\sigma_n^2)}{(\sigma_m^2-\sigma_n^2)} \tag{18}$$

where σ_n^2=noise energy; $\sigma_r^2=\sigma_m^2-\sigma_n^2$=real turbulent energy; and σ_m^2=measured turbulent energy. The ratio E quantifies the importance of estimating noise effects in high-energy flows. Each of the modeled spectra obtained from the simulation of different flow conditions is integrated up to the Nyquist frequency, in order to compute the turbulent flow energy for the specified flow conditions. This energy value is then compared with a noise energy computed using the white noise characteristics of the Doppler noise. The noise energy is obtained as the product of the noise energy level, E_{11n}, and the Nyquist frequency=$f_R/2$. Thus, the variables used in this part of the analysis are: U_c, L, η, E_{11n}, and f_R. A range of noise energy levels, 10^{-7} m^2/s$\leq E_{11n}\leq 10^{-5}$ m^2/s, typical of acoustic Doppler velocimeter measurements, is consid-

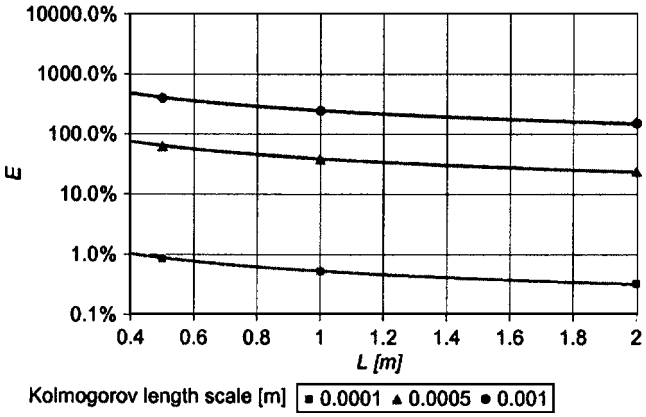

Fig. 15. Ratio between the noise energy and the real turbulent energy, E, for U_c=0.5 m/s, f_R=25 Hz, and $E_{11n}=10^{-5}$ m^2/s. Flow conditions with $L<0.4$ m ($F<20$) are disregarded in the analysis because of the requirements suggested by acoustic Doppler velocimeter performance curves.

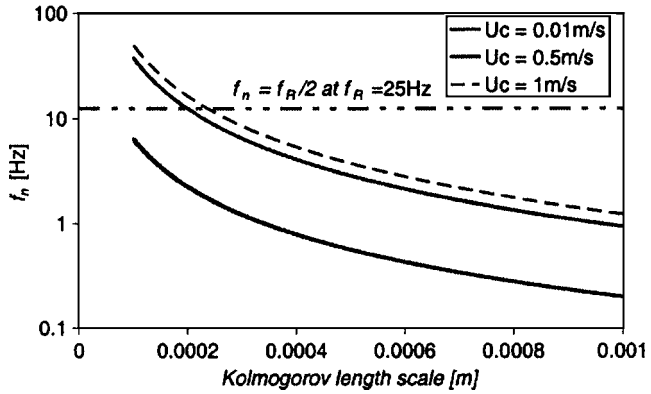

Fig. 17. Characteristic frequency f_n for f_R=25 Hz and $E_{11n}=10^{-5}$ m^2/s. The frequency f_n is defined as the frequency where the real flow energy is equal to the noise energy. Above this frequency, noise is the most important component in the measured power spectrum.

ered here based on experience and previous research (Nikora and Goring 1998).

The energy ratio E is plotted in Figs. 14–16 as a function of the Kolmogorov length scale, η, and the energy containing eddy length scale, L. The ratio E decreases as the energy-containing eddy length scale increases, while E increases as η increases (i.e., noise is less important for energetic flows). It was found that U_c is not a relevant parameter describing the behavior of E. As it was introduced before, a dimensionless number $F=f_R L/U_c>20$ is required to obtain a good description of the flow turbulence using acoustic Doppler velocimeters. For $F>20$, and the conditions represented in Figs. 14–16 (f_R=25 Hz and U_c=0.5 m/s), turbulent energy in flows with $L<0.4$ m will not be well resolved. Therefore, these conditions are not represented in these figures. Fig. 14 shows that the highest ratio E predicted for $\eta\leqslant 0.0005$ m (which is representative of most laboratory and field experiments) and the noise energy level $E_{11n}=10^{-6}$ m^2/s is 7%. For flows with $L>0.7$ m, E is lower than 5%. Fig. 16 shows that E is lower than 5% for all the possible flow conditions and instrument configurations which satisfy the APCs requirements at $E_{11n}=10^{-7}$ m^2/s. However, Fig. 15 ($E_{11n}=10^{-5}$ m^2/s) deserves special attention because for most conditions the ratio E remains at values higher than 10%, which indicates that the noise energy must be subtracted in these conditions because of its importance.

A complementary analysis included here is related to the definition of the characteristic frequency, f_n, for the flow conditions and instrument configuration cited before. Values of f_n smaller than the Nyquist frequency indicate that the flat plateau in the power spectrum can be detected. Using the fact that the measured energy power spectrum is the sum of the real energy spectrum and the noise spectrum (Nikora and Goring 1998), a set of measured energy spectra was built for the different flow conditions and noise energy level. The frequency f_n is defined as the frequency where the real flow energy is equal to the noise energy. Above this frequency, noise is the most important component in the measured power spectrum. The detected values of the fre-

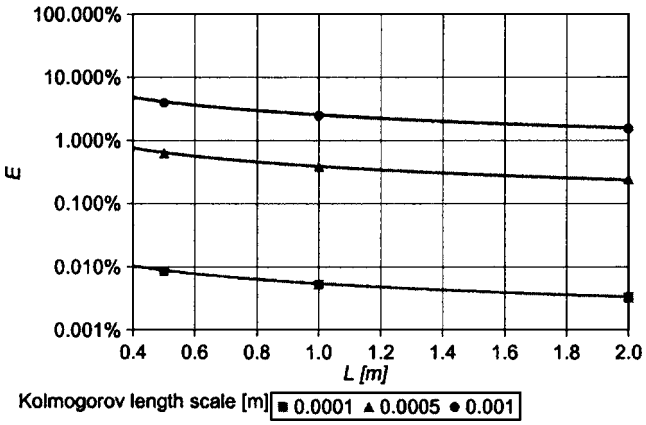

Fig. 16. Ratio between the noise energy and the real turbulent energy, E, for U_c=0.5 m/s, f_R=25 Hz, and $E_{11n}=10^{-7}$ m^2/s. Flow conditions with $L<0.4$ m ($F<20$) are disregarded in the analysis because of the requirements suggested by acoustic Doppler velocimeter performance curves.

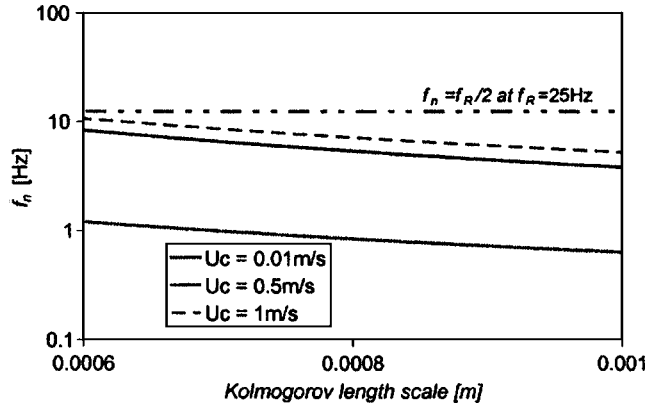

Fig. 18. The characteristic frequency f_n where the real flow energy is equal to the noise energy for f_R=25 Hz and $E_{11n}=10^{-6}$ m^2/s. The ratio E is lower than 10% for $\eta\leqslant 0.0006$ m (see Fig. 14). For $\eta>0.0006$ m, the noise energy is important and it must be corrected.

quency f_n are plotted in Figs. 17 and 18 as a function of the Kolmogorov length scales (η), for three different convective velocities (U_c). In this analysis, the eddy-containing eddy length scale, L, is not found to be a relevant parameter. The plots show that the higher the value of η, the smaller the frequency where noise is detected (recall that higher η implies a lower-energy flow). Additionally, it can observed that the larger U_c, the higher the value of the frequency f_n.

Fig. 17 shows the case that deserves most attention according to the analysis presented before ($E_{11n}=10^{-5}$ m^2/s) because it presents the highest ratio E (Fig. 15). For all of the flow conditions where $\eta > 0.00025$ m, the frequency f_n is lower than Nyquist frequency ($f_R/2$) if a user-defined sampling frequency $f_R=25$ Hz is used. It can be observed in Fig. 15 that the flow and sampling conditions satisfying the requirements imposed for the APC (resolving the flow turbulence) with $\eta < 0.00025$ m, are values of $E<10\%$. In cases where the ratio E is higher than 10% ($\eta > 0.00025$ m), the noise floor can be detected from the measured spectrum, and thus the spectral analysis technique to estimate the noise energy level can be used. For the value of noise energy level, $E_{11n}=10^{-6}$ m^2/s, the ratio E is lower than 10% for Kolmogorov length scales $\eta \leqslant 0.0006$ m (Fig. 14). Therefore, two regions can be defined in Fig. 18: For one of them ($\eta > 0.0006$ m) the noise energy is important and must be corrected. Only these conditions are represented in Fig. 18. For this entire region, $f_n < 12.5$ Hz. Thus, using a defined user sampling frequency $f_R=25$ Hz, the noise plateau will be observed in the spectrum.

It can be concluded that in the cases where the noise energy is important, in relation to the real turbulent energy of the signal, the noise energy level can be computed using the spectral analysis method because the white noise plateau is observed in the power spectrum (Figs. 15 and 17). In cases of very high-energy flows (or very small noise energy level), this method cannot be used, although the noise energy is smaller than 10% of the real total energy.

Conclusions

Acoustic Doppler velocimeters have proved to yield a good description of turbulence when certain conditions are satisfied. These restrictions are related to the instrument configuration (sampling frequency and noise energy level) and flow conditions (convective velocity and turbulence scales in the flow). In general, acoustic Doppler velocimeters produce a reduction in all of the even moments in the water velocity signal due to the low-pass filter used in the instrument. Additionally, this filter affects the autocorrelation functions (increasing *Rxx* for small lag times), the time scales computed from them (producing results that are high biased), and the power spectrum (producing a low resolution of the inertial range). However, the present analysis indicates that all of these effects are rather negligible in cases where a value of the dimensionless frequency $F=f_R L/U_c > 20$ is used. This result provides a new criterion to check the validity of the acoustic Doppler velocimeter measurements as a good representation of the turbulence in any flow with known convective velocity and length scales. The acoustic Doppler velocimeter should be operated at the maximum recording rate f_R so that F is as large as possible. However, it must be noted that the higher sampling frequency will produce a higher Doppler noise energy of the signal. The decision about the selected frequency to record data should thus optimize the values of F to make the recorded signal representative of the flow turbulence, but seek to keep the Doppler noise energy level of the signal as low as possible.

Doppler noise constitutes an important error source in acoustic Doppler turbulence measurements and its effects on the turbulence parameters computed from these signals must be quantified and removed in certain cases. The spectral analysis method provides the most realistic estimation of energy Doppler noise level. After the noise energy level is detected, noise effects must be subtracted from estimators of the power spectrum, variance, TKE, autocorrelation function, convective velocity, length and time scales, and rate of dissipation of TKE. However, the spectral analysis method cannot be used in high turbulent energy flows where the characteristic frequency f_n (where the noise is detected as a flat plateau in the spectrum) is higher than the Nyquist frequency. However, it is shown herein that in these cases, the Doppler noise contribution to the total measured energy is lower than 10%.

Acknowledgments

A number of federal and state agencies have supported several research projects leading to this work at the University of Illinois. They are the National Science Foundation, the Office of Naval Research, the U.S. Army Corps of Engineering, the U.S. Geological Survey, the U.S. Department of Agriculture, the Illinois Water Resources Center, the Illinois Department of Natural Resources, and the Metropolitan Water Reclamation District of Greater Chicago. The findings in this paper are the sole opinion of the writers and do not support or endorse any specific manufacturer of acoustic Doppler velocimeters. The writers thank Jim Best for his help in making the manuscript more readable as well as two anonymous reviewers for their constructive criticism.

Notation

The following symbols are used in this paper:

A_q = amplitude of weighted series cosines series;
B = flume width;
C = sound speed in water;
C_0 = parameter of the adopted spectrum function;
c_L, c_η = parameters of the adopted spectrum function;
d = diameter of the acoustic Doppler velocimeter's measurement volume;
d_R = diameter of the sampled volume set by the flow and sampling characteristics;
$d\phi/dt|_i$ = phase shift rate of the sound signal computed for the velocimeter's receiver i;
E = relative importance of the noise energy over the real turbulent energy;
$E_{11}(\kappa_1)$ = one-dimensional power spectrum function;
E_{11n} = noise energy level;
F = dimensionless parameter;
f = frequency;
f_{ADV} = sound signal frequency;
$f_{\text{cut-off}}$ = cut-off frequency of the digital filter;
f_L = shape function defined for the energy containing eddy part of the spectrum function;
f_n = characteristic frequency where noise is observed in power spectrum;

f_R = acoustic Doppler velocimeter's user-set frequency;
f_S = frequency of the three-dimensional velocity measurement process;
f_T = characteristic frequency of large eddies present in the flow;
f_η = shape function defined for the dissipation range of the spectrum function;
$H(f)$ = transfer function of the digital filter;
h = water depth;
j = $(-1)^{1/2}$;
L = energy containing eddy length scale;
N = number of values averaged in the signal to produce a digital signal with frequency f_R;
Ns = number of terms of the target spectrum used in the Shinozuka method;
Nt = number of samples in the generated synthetic time series;
p_0 = parameter of the adopted spectrum function;
Q = flow discharge;
Rxx = autocorrelation function;
T = time taken for an acoustic Doppler velocimeter to complete a three-dimensional velocity measurement;
T_{11} = time scale of the one-dimensional water velocity signal;
Tt = total simulated time in the synthetic signal;
t = time;
U_c = convective velocity;
U_i = mean flow velocity in the i direction;
u^* = shear velocity;
u_i' = fluctuation of the flow velocity in the i direction;
u_x, u_y, u_z = flow velocity vector components in the local Cartesian coordinate system;
v_i = flow radial velocity computed for each velocimeter receiver i (i=1,2,3);
$X(f)$ = Fourier transforms of the signal x;
x = signal sampled at f_S;
$Y(f)$ = Fourier transforms of the signal y;
y = signal obtained after digital averaging;
y_p = distance from the bottom of the flume;
α = amount of jitter in Shinozuka method;
β = parameter of the power spectrum function;
Δt = $1/f_S$;
Δt_x = $1/f_S$=interval between samples of signal x;
Δt_y = $1/f_R$=interval between samples of signal y;
ε = rate of dissipation of turbulent kinetic energy of the flow;
η = Kolmogorov length scale;
κ_1 = one-dimensional wave number;
ν = kinematic water viscosity;
σ = variance of the one-dimensional velocity signal;
σ_m = measured turbulent energy;
σ_n = noise energy;
σ_r = real turbulent energy;
τ_1, τ_2 = different pulse repetition rates for the acoustic Doppler velocimeter pulse-pair scheme;
τ_D = dwell time for the acoustic Doppler velocimeter pulse-pair scheme; and
ϕ = random phase angle of the synthetic flow velocity series;
$\omega_q, \omega_q', \Delta\omega$ = variables of the Shinozuka method.

References

Anderson, S., and Lohrmann, A. (1995). "Open water test of the Sontek acoustic Doppler velocimeter." *Proc., IEEE Fifth Working Conf. on Current Measurements*, IEEE Oceanic Engineering Society, St. Petersburg, Fla., 188–192.

Barkdoll, B. (2002). "Discussion of 'Mean flow and turbulence structure of open-channel flow through non-emergent vegetation,' by F. Lopez, and M. H. García." *J. Hydraul. Eng.*, 128(11), 1032.

Bendat, J., and Piersol, A. (2000). *Random data*. 3rd Ed., Wiley, New York.

Gordon, L., and Cox, J. (2000). "Acoustic Doppler velocimeter performance in a laboratory flume." *NortekUSA Technical Rep.*, Nortek USA, San Diego.

Hamming, R. (1983). *Digital filters*, 2nd Ed., Prentice Hall, Englewood Cliffs, New Jersey.

Heskestad, G. (1965). "A generalized Taylor hypothesis with application for high Reynolds number turbulent shear flows." *J. Appl. Mech.*, 32, 735–739.

Jeffries, W., Infield, D., and Manwell, J. (1991). "Limitations and recommendations regarding the Shinozuka method for simulating wind data." *Wind Eng.*, 15(3), 147–154.

Kraus, N. C., Lohrmann, A., and Cabrera, R. (1994). "New acoustic meter for measuring 3D laboratory flows." *J. Hydraul. Eng.*, 120(3), 406–412.

Lane, S., et al. (1998). "Three-dimensional measurement of river channel flow processes using acoustic Doppler velocimetry." *Earth Surf. Processes Landforms*, 23, 1247–1267.

Lemmin, U., and Lhermitte, R. (1999). "Discussion of 'ADV measurements of turbulence: Can we improve their interpretation?' by V. I. Nikora, and D. G. Goring." *J. Hydraul. Eng.*, 125(9), 987–988.

Lhermitte, R., and Serafin, R. (1984). "Pulse to pulse Doppler sonar signal processing techniques." *J. Atmos. Ocean. Technol.*, 1(4), 293–308.

Lohrmann, A., Cabrera R., and Kraus, N. (1994). "Acoustic Doppler velocimeter (ADV) for laboratory use." *Proc. Symp. on Fundamentals and Advancements in Hydraulic Measurements and Experimentation*, ASCE, New York, 351–365.

Lopez, F., and Garcia, M. H. (2001). "Mean flow and turbulence structure of open-channel flow through nonemergent vegetation." *J. Hydraul. Eng.*, 127(5), 392–402.

McLelland, S., and Nicholas, A. (2000). "A new method for evaluating errors in high-frequency ADV measurements." *Hydrolog. Process.*, 14, 351–366.

Mercier, R. (1984). "The reactive transport of suspended particles: Mechanisms and modeling." PhD thesis, Massachussets Institute of Technology, Cambridge, Mass.

Nezu, I., and Nakagawa, H. (1993). *Turbulence in open channel flows*, IAHR, Balkema, Rotterdam, The Netherlands.

Nikora, V. I., and Goring, D. G. (1998). "ADV measurements of turbulence: Can we improve their interpretation?" *J. Hydraul. Eng.*, 124(6), 630–634.

Pope, S. (2000). *Turbulent flows*, Cambridge University Press, Cambridge, U.K.

Roy, A., Biron, P., and Lapointe, M. (1997). "Implications of low-pass filtering on power spectra and autocorrelation functions of turbulent velocity signals." *Math. Geol.*, 29(5), 653–668.

SonTek. (1997). "Pulse coherent Doppler processing and the ADV Correlation." *SonTek Tech. Note*, San Diego.

Shinozuka, M., and Jan, C. (1972). "Digital simulation of random processes and its applications." *J. Sound Vib.*, 25(1), 111–128.

Sreenivasan, K., Chambers, A., and Antonia, R. (1978). "Accuracy of moments of velocity and scalars fluctuations in the atmospheric surface layer." *Boundary-Layer Meteorol.*, 14, 341–359.

Voulgaris, G., and Trowbridge J. (1998). "Evaluation of the acoustic Doppler velocimeter (ADV) for turbulence measurements." *J. Atmos. Ocean. Technol.*, 15(1), 272–288.